Weighted-superposition approximation for x-ray and neutron reflectance

Xiao-Lin Zhou and Lei He
Department of Nuclear Engineering, 214 Nuclear Engineering Laboratory, University of Illinois at Urbana-Champaign, 103 South Goodwin Avenue, Urbana, Illinois 61801
(Received 20 December 1993)

An approximate formula is derived for the x-ray and neutron reflectance of a one-dimensional scattering-length-density (SLD) profile based on the principle of superposition of the wave field. The SLD profile is regarded as being composed of an infinite number of histogramlike differential SLD steps which are distributed along the depth direction. A simple Fresnel reflection is assumed to occur at each differential step. The elemental Fresnel reflections from all the differential steps, weighted by their respective propagation effects, add up to the overall reflectance of the one-dimensional SLD profile in the form of an integral. The reflectance obtained this way is shown to reduce to the Born approximation for large-wave-vector transfer Q and to the modified Born approximation for very thin surface structures. The accuracy of the formula is evaluated through comparisons with Parratt's recurrence formula, the Born approximation, and the distorted-wave Born approximation (DWBA) for a few selected SLD profiles imitating actual experimental SLD profiles. It is concluded that the formula is, in general, more accurate than the Born and DWBA approximations and is valid in the entire range of wave-vector transfer Q except slight deviations in the narrow region around the total reflection edge. The formulation also applies to absorptive materials when the SLD profile is taken to be complex. Owing to the high accuracy and simplicity of the formula, a scheme is proposed to use the formula for the reconstruction of the SLD profile from measured reflectance and reflectivity data.

PACS number(s): 61.12.−q, 02.50.−r, 68.10.−m, 02.70.−c

I. INTRODUCTION

The reflection of x rays and neutrons by a stratified film obeys a one-dimensional wave equation [1] with a propagation wave number which depends on the vertical scattering-length-density (SLD) profile of the sample. From such an equation, an open-form solution for the reflectance can be obtained using the standard Green's-function approach [2–4]. The open-form expression for the reflectance contains an unknown wave function in the region of the film, and one has to approximate the unknown wave function. The simplest choice of the wave function is the Born approximation [5], which assumes that the reflection is low so the incident wave is essentially unchanged inside the film. A more consistent approximation is the distorted-wave Born approximation (DWBA) [6], which uses the wave function of a reference film (say a uniform average film) for the unknown wave function in the actual film. The Born approximation is valid for very thin films or for arbitrary films only at large Q values. The DWBA works well for thin films of which the SLD profiles can be closely approximated by simple profiles such as a uniform layer. For a more general sample, say a thick diffused interfacial region, both the Born and DWBA break down and better approximations are needed. One such approximation is the so-called small curvature approximation (SCA) given in [2], which was proven to reduce to and be more accurate than both Born and DWBA. An even better approximation called the modified WKB (MWKB) approximation was given in [4], where a uniform-layer Green's function was employed, and the wave function inside the sample was treated by modifying the WKB approximation [7]. The above approximations are all based on Green's functions and they differ in forms and physical contents. In the following, we present another approach to calculate the reflectance, namely the weighted superposition approximation (WSA). The essence of the method is the principle of superposition of the wave field as commonly used in the electromagnetic-field theory. This approximation is unique because it is simple in principle yet more accurate than all other approximations, and most importantly can be used to reconstruct the SLD profile from measured reflectance or reflectivity data.

II. THE WEIGHTED SUPERPOSITION APPROXIMATION (WSA)

A plane wave (x ray or neutron) is assumed to impinge on a stratified sample with a SLD profile $\rho(z)$ as illustrated in Fig. 1. The sample occupies the region $(-d,0)$, the substrate (or bulk), the region $(0,\infty)$, and the incident space of air $(-\infty,-d)$. For the derivation of the WSA, the sample SLD profile $\rho(z)$ is treated as composed of an infinite number of histogramlike small differential SLD steps distributed along the depth direction z. A simple elemental Fresnel reflection is assumed to occur at each of the steps. The weighted superposition of all the elemental Fresnel-reflected wavelets constitutes the reflectance from the entire sample. The weight for each elemental Fresnel reflection is a factor that accounts for the accumulated phase and attenuation of the amplitude of the wave both before and after the reflection at a differential step. As will be seen below, this treatment

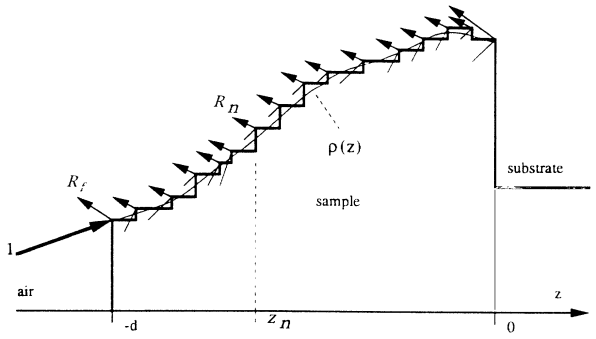

FIG. 1. Illustration of the superposition of elemental Fresnel reflections from the differential steps in the SLD profile of a stratified sample. The number "1" in the figure indicates the unit amplitude of the incident wave. R_f is the Fresnel reflectance of the front surface of the sample. R_n denotes the Fresnel reflectance of the differential SLD step at z_n. The arrows represent the elemental Fresnel-reflected wavelets. Since wavelets from different positions z_n have to traverse different ranges of the sample before reaching the incident space, they should be weighted differently according to their respective propagation effects as given by Eq. (5) in order to add up correctly to the total reflectance of the sample.

will lead to very simple and accurate formulas in a straightforward manner.

A. Derivation of the WSA

For the reflection from a film situated on top of a substrate, the film-substrate combination can be regarded as being composed of two parts: the air-film interface and the rest. The reflected wave from the air-film interface interferes with that from the rest of the medium (namely, film plus substrate minus air-film interface) to result in oscillations in the reflectivity-Q curve. This interference comes in the form of multiple reflections. To properly account for this effect, we choose to treat the front air-film interface and the rest separately, and then combine their contributions to obtain a composite multiple-reflection solution. The front air-film interface has a Fresnel reflectance given by

$$R_f=\frac{k_0-k_f}{k_0+k_f},\quad k_f=\sqrt{k_0^2-4\pi\rho_f}\ , \tag{1}$$

where $\rho_f=\rho(-d)$ and $k_0=(2\pi/\lambda)\sin\theta$, with λ denoting the wavelength and θ the grazing angle of incidence. The reflection from the rest of the medium includes the region from $z=-d^+$ to $z=\infty$. This means that it includes the entire film-substrate medium except the air-film interface. Suppose the reflection of the medium is denoted by r_m, then the combined reflection of the air-film interface and the film medium is, according to Parratt's formula [8],

$$r=\frac{R_f+r_m}{1+R_f r_m}\ , \tag{2}$$

the squared modulus of which is the reflectivity measured in experiments. The medium reflection r_m excluding the front air-film interface can be calculated as follows. The elemental Fresnel reflection at the differential step at z_n is given by

$$R_n=\frac{k(z_n-\Delta z/2)-k(z_n+\Delta z/2)}{k(z_n-\Delta z/2)+k(z_n+\Delta z/2)}\ . \tag{3}$$

As $k(z)=\sqrt{k_0^2-4\pi\rho(z)}$, the Fresnel reflectance R_n in Eq. (3) approaches the following limit when Δz approaches an infinitesimally small value of dz:

$$\lim_{\Delta z\to dz} R_n=\frac{\pi(d\rho/dz)}{k^2}dz\ . \tag{4}$$

The weight factor for the elemental Fresnel reflection at z_n is given by

$$W(z_n)=\exp\left[2i\int_{-d}^{z_n}k(z)dz\right]\ . \tag{5}$$

Multiplying Eq. (4) by Eq. (5), summing the product over n, and taking the limit that the number of points n approaches infinity, one obtains

$$r_m=\pi\int_{-d^+}^{\infty}dz\frac{d\rho/dz}{k^2}\exp\left[2i\int_{-d}^{z}k(z)dz\right]\ . \tag{6}$$

Here $-d^+$ means the integration begins on the plus side of $z=-d$. Combining Eqs. (1), (2), and (6) and considering the fact that Eq. (6) equals R_f if the integration limits $(-d^+,\infty)$ are replaced by $(-d^-,-d^+)$, we obtain

$$r=\frac{\pi\int_{-d}^{\infty}dz\frac{d\rho/dz}{k^2}\exp\left[2i\int_{-d}^{z}k(z)dz\right]}{1-R_f^2+\pi R_f\int_{-d}^{\infty}dz\frac{d\rho/dz}{k^2}\exp\left[2i\int_{-d}^{z}k(z)dz\right]}\ , \tag{7}$$

$$k(z)=\sqrt{k_0^2-4\pi\rho(z)}\ , \tag{8}$$

where the integration limits $(-d,\infty)$ include the air-film interface.

More generally, if $-d$ in the integration limits is extended in the negative direction to include the front surface such that $\rho(-d)=0$, Eq. (1) gives $R_f=0$, and Eq. (7) reduces to

$$r=\pi\int_{-d}^{\infty}dz\frac{d\rho/dz}{k^2}\exp\left[2i\int_{-d}^{z}k(z)dz\right]\ . \tag{9}$$

Equation (9) has a very simple form yet will be shown still to be very accurate as the correct phase relation Eq. (5) has been included. We point out that Eq. (7) approaches Eq. (9) when the front surface becomes gentle and smooth, and only a small difference occurs when the front surface of the SLD profile is sharp. It is noted that the reflectance Eq. (9) is a simple generalization of the Born approximation, because replacing the phase $2k_0z$ in the Born approximation by $\int 2k(z)dz$ directly leads to Eq. (9).

It is observed from Eq. (9) that the reflectance r is related to the SLD in a nonlinear way, such that the reflectance r is not equal to a Fourier transform of the gradient of the SLD. However, at large Q, k approaches the free-space value k_0, making Eq. (9) a real Fourier transform similar to the diffraction amplitude [9] in crys-

tallography. At small and intermediate k_0, the SLD seriously affects k and the phase factor in the exponential term in Eq. (9). The phase for positive SLD values is smaller than the free-space value. As a result, the nonlinearity comes about owing to a phase shift (or phase lagging) caused by the SLD. This is a significant effect, as it is well known that the interference of wavelets from various locations inside the SLD profile depends very sensitively on their relative phases.

B. Reduction of WSA to Born, modified Born, and free-liquid approximations

At large wave-vector transfer Q, the wave number k reduces to the free-space wave number k_0. Both Eqs. (7) and (9) reduce to

$$r=\frac{\pi}{k_0^2}\int_{-d}^{\infty}dz\frac{d\rho}{dz}e^{2ik_0z}=\frac{4\pi}{Q^2}\int_{-d}^{\infty}dz\frac{d\rho}{dz}e^{iQz}\ , \tag{10}$$

which is the Born approximation [2]. Note that Q is the wave-vector transfer $Q=2k_0$, and a constant phase e^{iQd} is omitted from Eq. (10).

For a free-liquid surface with a thin surface structure, say 200 Å thick, the k in the denominator in Eq. (9) can be approximated by the value at the air-film interface, i.e.,

$$k\approx\frac{k_0+k_b}{2}\ , \tag{11}$$

and one automatically obtains from Eq. (9) that

$$r=\frac{R_b}{\rho_b}\int_{-d}^{\infty}dz\frac{d\rho}{dz}\exp\left[2i\int_{-d}^{z}k(z)dz\right]\ , \tag{12}$$

where ρ_b and R_b, respectively, are the SLD and the Fresnel reflectance of the bulk liquid. This formula can be used to calculate the reflectance of a free-liquid surface of a few hundred Å, and is called the free-liquid approximation.

If the free-liquid surface has an extremely thin structured surface region (<50 Å), Eq. (12) can be further reduced if one approximates the phase by $\exp(2ik_0z)$. Then

$$\frac{r}{R_b}=\frac{1}{\rho_b}\int_{-d}^{\infty}dz\frac{d\rho}{dz}e^{iQz}\ , \tag{13}$$

which is identical to the modified Born approximation given in [10] for very thin liquid surfaces. This result could also be obtained from Eq. (10) by forcing Eq. (10) to equal the Fresnel reflectance R_b for a sharp interface. Note that Eq. (13) applies to only very thin structures of <50 Å, while Eq. (12) could be applied to free liquids with surface structures as thick as a few hundred Å.

III. NUMERICAL COMPARISONS

We evaluate the validity of Eqs. (7) and (9) by comparing them numerically with Parratt's recurrence formula and the Born and DWBA approximations for a few SLD profiles. The profiles are labeled from (a) to (g) and their functional forms are listed in Table I.

Profiles (a)–(g) in Table I are plotted in Figs. 2(a)–2(g), respectively, with the proper substrate SLD's indicated. For generality and practicality, profiles (a)–(c) are chosen to represent increasing functions, profile equations (d)–(f) decreasing functions, and profile equation (g) a nonmonotonic function. Figure 2(a) resembles the surface SLD profile of a diffused protonated hydrocarbon layer on top of a deuterated hydrocarbon bulk [11]. Figure 2(b) simulates the surface density of some liquids which starts from

TABLE I. Scattering-length-density profiles used for evaluating Eqs. (7) and (9). The profile numbers (a) to (g) correspond to plots (a) to (g) in Fig. 2.

Profile no.	Range of z (Å)	Functional form of $\rho(z)$ (Å^{-2})
(a)	$-500\le z\le 0$	$-0.5\times10^{-6}+3.5\times10^{-6}\left[1+\int_0^{z+250/100}e^{-u^2}du\right]$
(b)	$-1000\le z\le 0$	$6.5\times10^{-9}(z+1000)+1.0\times10^{-6}\sin\left[\frac{2\pi(z+1000)}{235}\right]$
(c)	$-1000\le z\le 0$	$2.0\times10^{-6}+4.0\times10^{-6}\exp\left[-\frac{1}{2}\left[\frac{z+100}{200}\right]^2\right]$
(d)	$-1000\le z\le 0$	$2.0\times10^{-6}+3.0\times10^{-6}\exp\left[-\frac{z+100}{300}\right]$
(e)	$-1000\le z\le 0$	$2.5\times10^{-6}+2.5\times10^{-6}\exp\left[-\frac{z+1000}{300}\right]\sin\left[\frac{2\pi(z+1000)}{150}\right]$
(f)	$-2000\le z\le 0$	$1.5\times10^{-6}+2.5\times10^{-6}\left[1-\int_0^{z+1000/200}e^{-u^2}du\right]$
(g)	$-1000\le z\le 0$	$4.0\times10^{-6}+2.5\times10^{-6}\cos\left[\frac{2\pi(z+900)}{800}\right]$

air and increases oscillatorilly to the bulk level. Figure 2(c) mimics the neutron SLD profile of a polymer blend with a Gaussian adsorption profile at the substrate surface. Figure 2(d) is a typical exponential adhesion profile corresponding to the Cahn model. Figure 2(e) is a damped oscillatory density profile found in liquid crystals, microemulsions [12], and some liquid metals. Figure 2(f) is representative of an interdiffused polymer bilayer [13]. Figure 2(g) resembles a trilayer with diffused interfaces.

Figures 3–9 are the reflectivities calculated from Eq. (9) for the profiles Figs. 2(a)–2(g) in comparison with Parratt's recurrence formula and the Born approximation [Eq. (10)]. The calculated reflectivities from Eq. (9) are plotted in solid lines, Parratt's formula in circles, and the Born approximation [Eq. (10)] in dotted lines. In Fig. 3,

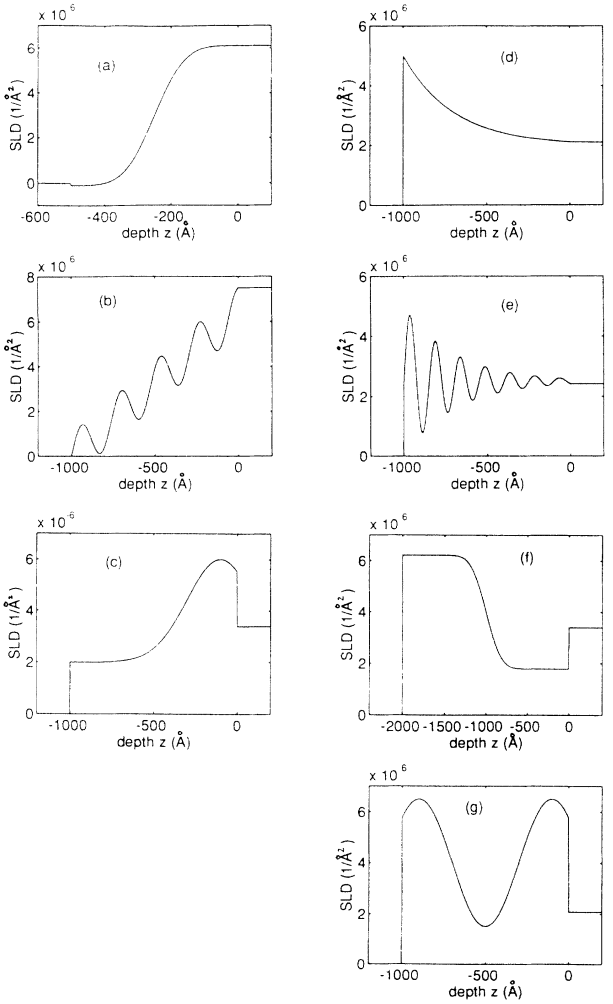

FIG. 2. Plots of seven SLD profiles listed in Table I. They are chosen for the comparison of Eqs. (7) and (9) with Parratt's formula and the Born and DWBA approximations. Plots (a)–(c) represent increasing SLD profiles, plots (d)–(f) are decreasing profiles, and plot (g) is a nonmonotonic SLD profile. They combine to cover a range of functional characteristics wide enough to represent most experimental SLD profiles in neutron and x-ray reflectometry.

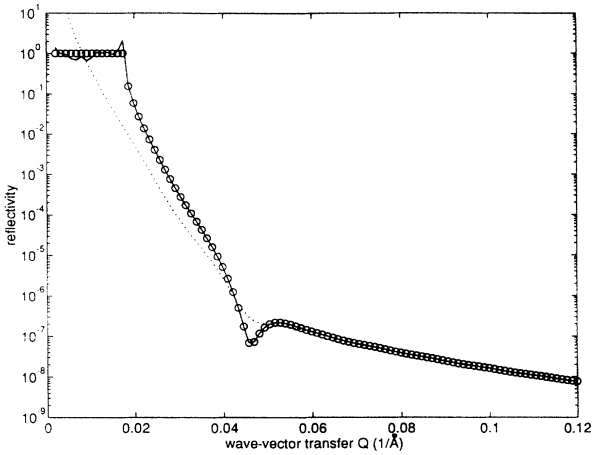

FIG. 3. Comparison of the reflectivity calculated from Eq. (9) with those from Parratt's recurrence formula and the Born approximation [Eq. (10)] using the SLD profile [Fig. 2(a)]. The circles are Parratt's result, the solid line is from Eq. (9), and the light dotted line is for the Born approximation.

the solid line from Eq. (9) goes right through the circles for Parratt's result except for small deviations on the total reflection plateau. The Born approximation is incorrect by a few orders of magnitude at small Q values, but approaches the correct result as Q increases. In Figs. 4–9, the same comparison is observed. Comparisons of the calculations for seven different SLD profiles have led us to believe that in general Eq. (9) agrees with Parratt's exact result within 2% except for small deviations around the critical plateau. As the deviations are small with respect to experimental data fluctuations in x-ray and neutron reflectometry, the small errors are not expected to degrade the validity of Eq. (9) if it is used to perform data analyses. That means that Eq. (9) can be regarded

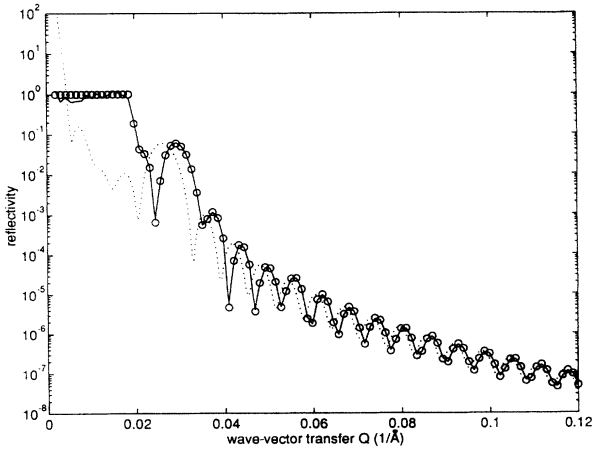

FIG. 4. Comparison of the reflectivity calculated from Eq. (9) with those from Parratt's recurrence formula and the Born approximation [Eq. (10)] using the SLD profile [Fig. 2(b)]. The circles are Parratt's result, the solid line is from Eq. (9), and the light dotted line is for the Born approximation.

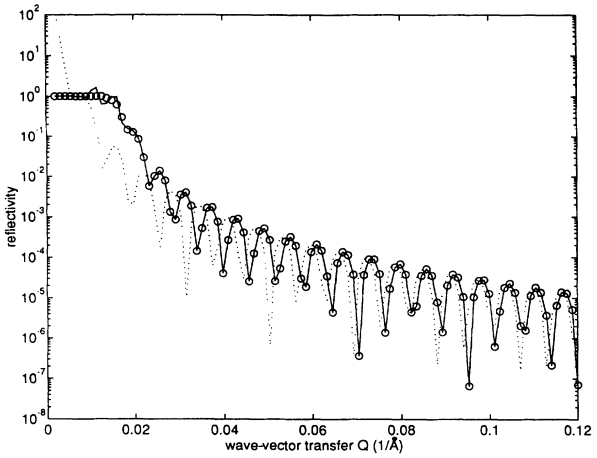

FIG. 5. Comparison of the reflectivity calculated from Eq. (9) with those from Parratt's recurrence formula and the Born approximation [Eq. (10)] using the SLD profile [Fig. 2(c)]. The circles are Parratt's result, the solid line is from Eq. (9), and the light dotted line is for the Born approximation.

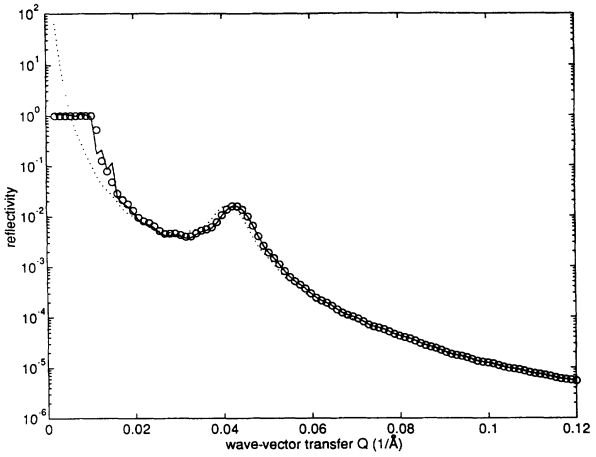

FIG. 7. Comparison of the reflectivity calculated from Eq. (9) with those from Parratt's recurrence formula and the Born approximation [Eq. (10)] using the SLD profile [Fig. 2(e)]. The circles are Parratt's result, the solid line is from Eq. (9), and the light dotted line is for the Born approximation.

as an accurate formula for the reflectance. The Born approximation is strictly a large-Q approximation and is correct only at large-Q values. We point out that the total reflection plateau is approximately reproduced by Eq. (9) in all cases from Figs. 3 to 9, and this is significant because most known approximations cannot achieve this for the different types of SLD profiles in Figs. 2(a)–2(g).

Equation (7) has a more complex form than Eq. (9), and is expected to be more accurate than Eq. (9) when the air-film interface is sharp. When the air-film interface is very gentle and smooth, R_f tends to zero and Eq. (7) approaches Eq. (9). To confirm this, we performed similar calculations of Eq. (7), and the results are plotted in Figs. 10–16. In these figures, the DWBA as given by Eq. (2.6c) in [4] is also calculated for comparison, and is given by the thicker black dots. The circles are Parratt's formula, the solid lines are Eq. (7), and the dotted lines are the Born approximation [Eq. (10)]. Figure 13 is for the exponential profile with a very sharp front surface. It shows that the solid line from Eq. (7) is almost identical to the circles from Parratt's formula. If one checks the corresponding figure for Eq. (9), i.e., Fig. 6, it can be seen that Eq. (7) is more accurate than Eq. (9). However, if one compares Eqs. (7) and (9) through all the other figures, the difference is marginal and can be neglected as far as data analyses are concerned.

In Fig. 10 for the profile in Fig. 2(a), the solid line from Eq. (7) goes right through every circle from Parratt's for-

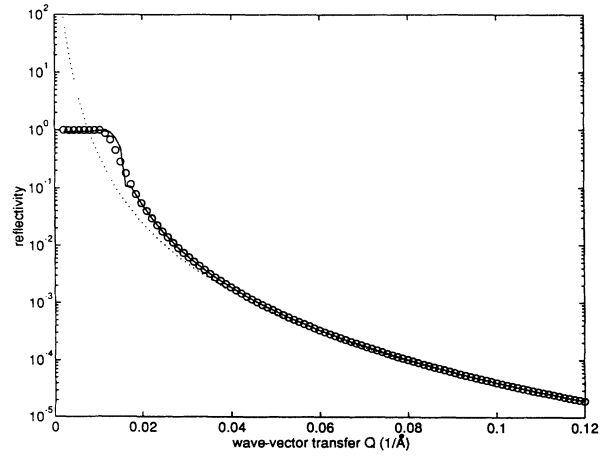

FIG. 6. Comparison of the reflectivity calculated from Eq. (9) with those from Parratt's recurrence formula and the Born approximation [Eq. (10)] using the SLD profile [Fig. 2(d)]. The circles are Parratt's result, the solid line is from Eq. (9), and the light dotted line is for the Born approximation.

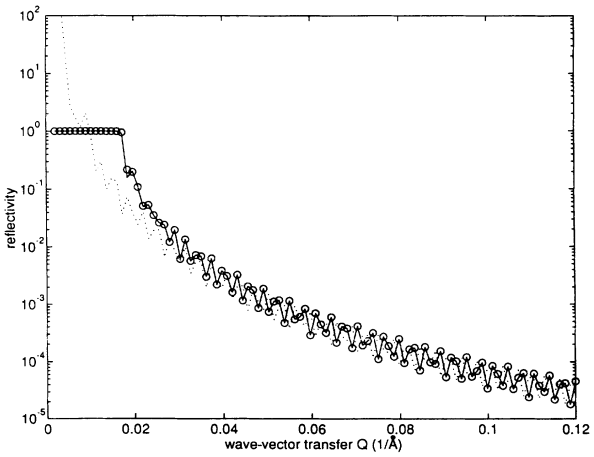

FIG. 8. Comparison of the reflectivity calculated from Eq. (9) with those from Parratt's recurrence formula and the Born approximation [Eq. (10)] using the SLD profile [Fig. 2(f)]. The circles are Parratt's result, the solid line is from Eq. (9), and the light dotted line is for the Born approximation.

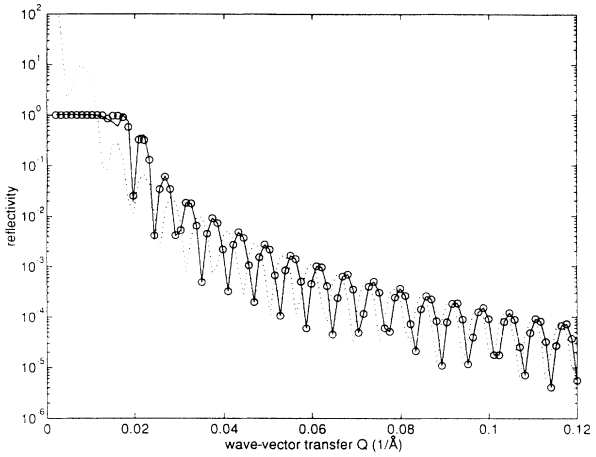

FIG. 9. Comparison of the reflectivity calculated from Eq. (9) with those from Parratt's recurrence formula and the Born approximation [Eq. (10)] using the SLD profile [Fig. 2(g)]. The circles are Parratt's result, the solid line is from Eq. (9), and the light dotted line is for the Born approximation.

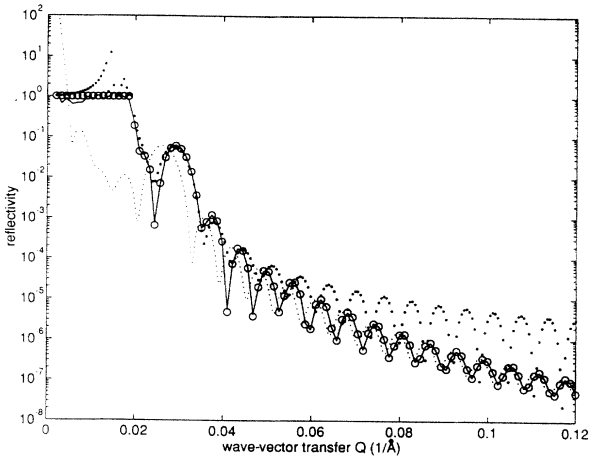

FIG. 11. Comparison of the reflectivity calculated from Eq. (7) with those from Parratt's recurrence formula, the DWBA, and the Born approximation [Eq. (10)] using the SLD profile [Fig. 2(b)]. The circles are Parratt's result, the solid line is from Eq. (7), the black dots are for the DWBA, and the light dotted line is for the Born approximation.

mula except the critical plateau. The Born approximation is again as in Fig. 3. The DWBA is correct for $Q=0.02-0.04$, but is completely different from Parratt's result at large-Q values. This is because the SLD in Fig. 2(a) cannot be well approximated by an average film across the interface. As a whole, Eq. (7) is found to be more accurate than the DWBA. Figures 11–16 show the same comparison, except that the DWBA gives accurate results for some profiles which can be well approximated by an average film. The best examples are Figs. 13 and 14. In Figs. 12–16, the DWBA's are found to be more accurate than the Born approximation but less accurate than the Born approximations in Figs. 10 and 11. This means that the DWBA is more accurate than the Born approximation for SLD profiles which are well approximated by an average SLD level, and less accurate for SLD profiles which are not. In addition, Figs. 12–16 also indicate that the DWBA approaches Eq. (7) and Parratt's formula as Q increases. In fact, at very large-Q values, all four curves merge together. The comparisons show that Eq. (7) is systematically more accurate than both the Born approximation and the DWBA, that Eqs. (7) and (9) are almost equally accurate, and that they both approximately reproduce the total reflection plateaus in the reflectivity curves. Furthermore, Eqs. (7) or (9) are accu-

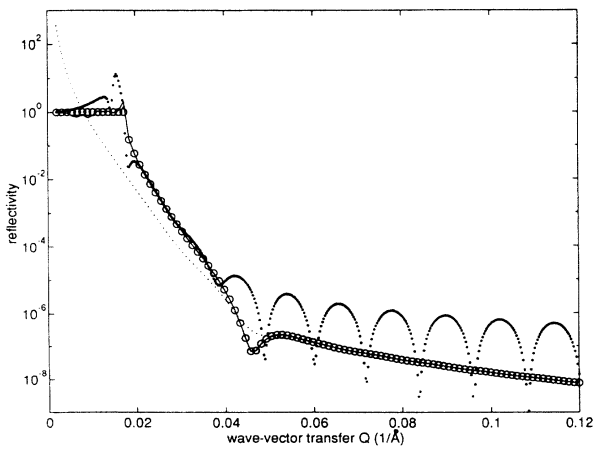

FIG. 10. Comparison of the reflectivity calculated from Eq. (7) with those from Parratt's recurrence formula, the DWBA, and the Born approximation [Eq. (10)] using the SLD profile [Fig. 2(a)]. The circles are Parratt's result, the solid line is from Eq. (7), the black dots are for the DWBA, and the light dotted line is for the Born approximation.

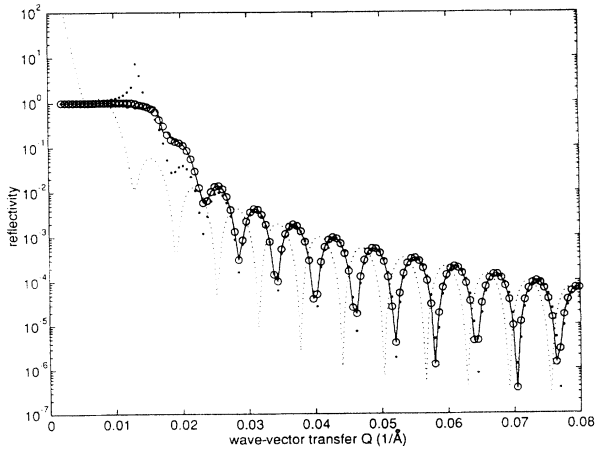

FIG. 12. Comparison of the reflectivity calculated from Eq. (7) with those from Parratt's recurrence formula, the DWBA, and the Born approximation [Eq. (10)] using the SLD profile [Fig. 2(c)]. The circles are Parratt's result, the solid line is from Eq. (7), the black dots are for the DWBA, and the light dotted line is for the Born approximation.

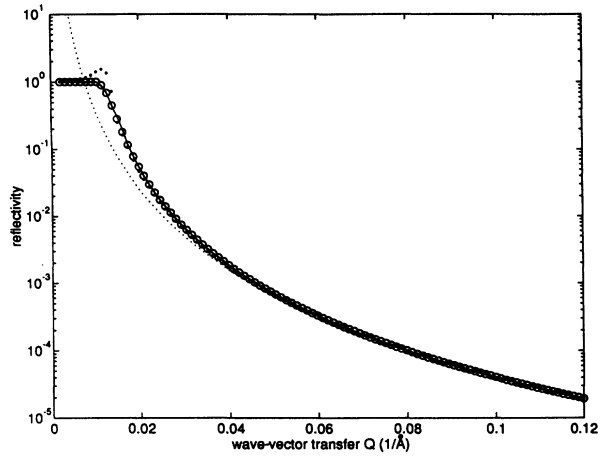

FIG. 13. Comparison of the reflectivity calculated from Eq. (7) with those from Parratt's recurrence formula, the DWBA, and the Born approximation [Eq. (10)] using the SLD profile [Fig. 2(d)]. The circles are Parratt's result, the solid line is from Eq. (7), the black dots are for the DWBA, and the light dotted line is for the Born approximation.

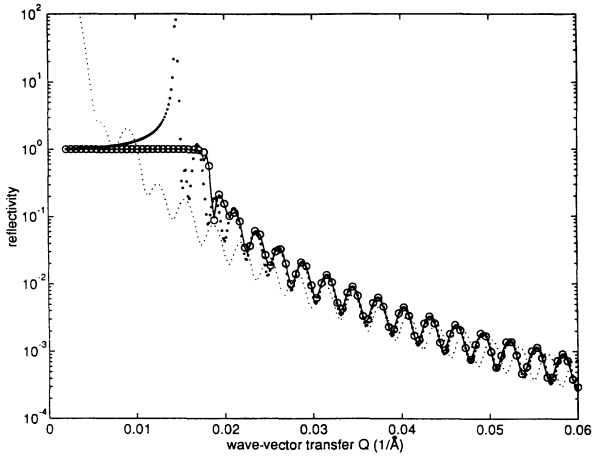

FIG. 15. Comparison of the reflectivity calculated from Eq. (7) with those from Parratt's recurrence formula, the DWBA, and the Born approximation [Eq. (10)] using the SLD profile [Fig. 2(f)]. The circles are Parratt's result, the solid line is from Eq. (7), the black dots are for the DWBA, and the light dotted line is for the Born approximation.

rate regardless of the functional shapes of the SLD profiles.

IV. USING WSA FOR SLD RECONSTRUCTION

The WSA formulas Eqs. (7) and (9) can be used to construct schemes to determine the SLD profile from measured data. This was demonstrated in [3] using another approximate formula. An iterative inversion algorithm can be developed based on Eqs. (7) or (9). Equations (7) and (9) can be rewritten as

$$I(r,\rho)=\int_{-d}^{0} dz \frac{d\rho}{dz}\Gamma(z,\rho) , \tag{14}$$

$$\Gamma(z,\rho)\equiv\frac{1}{k^2}\exp\left[2i\int_{-d}^{z}k(z)dz\right] , \tag{15}$$

$$I(r,\rho)\equiv\begin{cases}\dfrac{r}{\pi} & \text{for Eq. (9)}\\ \dfrac{r}{\pi}\dfrac{1-R_f^2}{1-rR_f} & \text{for Eq. (7) .}\end{cases} \tag{16}$$

Integrating the product of Eq. (14) with $\exp(-2ik_0z)$ over a range of k_0 from k_1 to k_2, we obtain an integral equation of the following form:

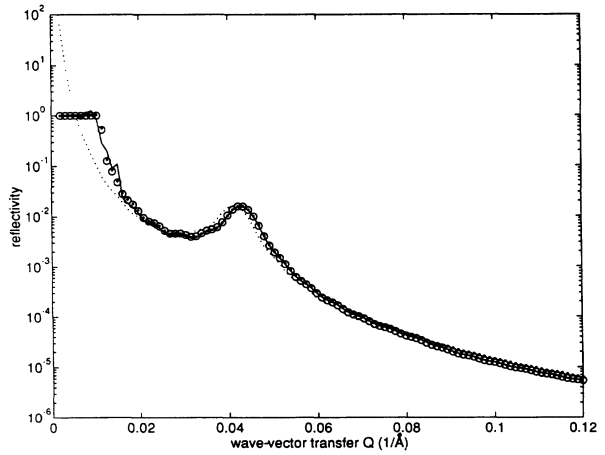

FIG. 14. Comparison of the reflectivity calculated from Eq. (7) with those from Parratt's recurrence formula, the DWBA, and the Born approximation [Eq. (10)] using the SLD profile [Fig. 2(e)]. The circles are Parratt's result, the solid line is from Eq. (7), the black dots are for the DWBA, and the light dotted line is for the Born approximation.

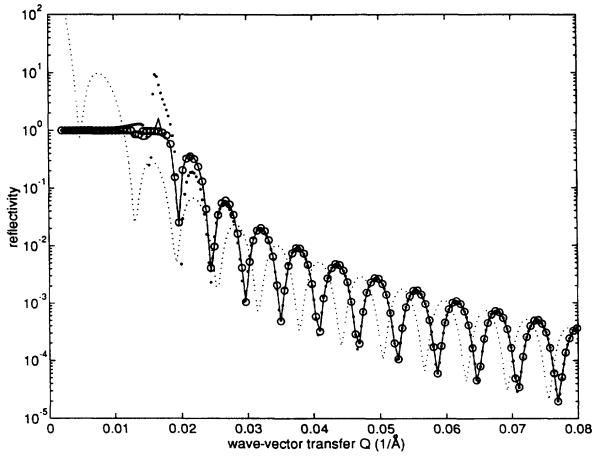

FIG. 16. Comparison of the reflectivity calculated from Eq. (7) with those from Parratt's recurrence formula, the DWBA, and the Born approximation [Eq. (10)] using the SLD profile [Fig. 2(g)]. The circles are Parratt's result, the solid line is from Eq. (7), the black dots are for the DWBA, and the light dotted line is for the Born approximation.

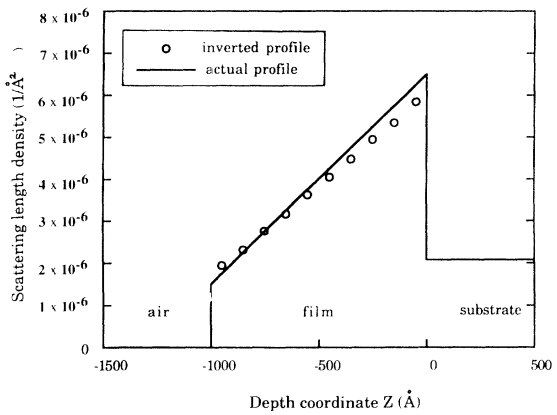

FIG. 17. The inverted SLD profile obtained via Eq. (21) from simulated reflectance data of a linear SLD profile. The solid line is the original profile, and the circles are the reconstructed result.

$$C(z)=\int_{-d}^{0} dz' \frac{d\rho(z')}{dz'} W(z',z) , \tag{17}$$

where $C(z)$ and the kernel $W(z',z)$, respectively, are the integration of the products of $\exp(-2ik_0z)$ with Eqs. (16) and (15) over k_0 from k_1 to k_2. We divide the spatial range $(-d,0)$ into N segments, with the nth segment spanning an interval from z_{n-1} to z_n, and the derivative of scattering length density in this interval is taken to be a constant ρ_n. Using Galerkin's method [14], we transform Eq. (17) into a matrix equation:

$$[C_m]=[W_{mn}][\rho_n] , \tag{18}$$

$$C_m=\int_{z_{m-1}}^{z_m} dz C(z) , \tag{19}$$

$$W_{mn}=\int_{z_{n-1}}^{z_n} dz' \int_{z_{m-1}}^{z_m} dz\, W(z',z) . \tag{20}$$

An iterative scheme calculates the jth value ρ_n^j from the $(j-1)$th values ρ_n^{j-1} by using the matrix inversion formula

$$[\rho_n^j]=[W_{mn}(\rho_n^{j-1})]^{-1}[C_m(\rho_n^{j-1})] . \tag{21}$$

The initial guess ρ_n^0 for the iteration can be chosen in such a way as to minimize the computation time.

Application of Eqs. (21) and (9) to one set of simulated reflectance data produced an approximate inverted scattering length density profile, as plotted with circles in Fig. 17 together with the input profile. The inverted profile is a close approximation of the input profile. Note that this is only a test case, and more work is in order for obtaining a method applicable to arbitrary SLD profiles. Rough as it is, Fig. 17 preliminarily demonstrates how the WSA may be used to invert reflection data in addition to revealing the nonlinear relationship between r and the SLD.

V. DISCUSSION

In this paper, the principle of superposition of the wave field has been successfully used to derive an approximate closed-form formula Eq. (9) for calculating the reflectance of a stratified sample characterized by a SLD profile $\rho(z)$. This treatment of x-ray reflection was based on the fact that x rays are electromagnetic waves, and electromagnetic fields obey the superposition principle. This principle also applies to neutron waves and acoustic waves because they are similar to x rays in that their wave equations are all linear. As a matter of fact, the superposition principle is a direct consequence of the linearity of the wave equations satisfied by the wave functions. This guarantees that the use of the superposition principle in this paper is physically legitimate. Because the principle of superposition is simple, the formulas are obtained in a straightforward fashion and are very simple in form compared to other formulations such as the Green's-function solution.

The formula Eq. (9) was shown to reduce to the Born approximation in the large-Q limit and the modified Born approximation for very thin liquid surfaces. Equation (9) also produces a new formula Eq. (12) for thin liquid surfaces which may be too thick (say 300 Å) to be accurately described by Eq. (13). For arbitrary films, the Born approximation failed in the low-Q region because, contrary to the assumption of weak reflection, the incident wave was modified significantly by the film. On the contrary, Eq. (9) is accurate because the exponential term inside the integral represents the correct propagation effect. The propagation effect has two parts: the phase change and the amplitude attenuation, both of which are represented very well by Eq. (5). Away from the critical edge, the wave propagates in the film with little attenuation, and the major factor is the phase shift as given in Eq. (5). Below the critical edge, the wave number k may become imaginary, and Eq. (5) predicts exponential attenuation, and the wave may become evanescent. In the vicinity of the total reflection edge, the wave may be propagating in some part of the sample while being attenuated in some other part of the sample. This complexity makes it difficult to calculate the amplitude change very accurately and causes errors. As a whole, Eq. (9) is found to be valid over the entire range of wave-vector transfer Q except for small errors in the vicinity of the total reflection edge.

From the formula Eq. (9), one sees most directly that the nonlinear dependence of the reflectance on the SLD profile of the sample is through the phase factor. This is an important understanding for reflectivity data analyses. Besides being the simplest and most accurate approximate reflectance formula, Eq. (9) may be used to perform data inversion as described in Sec. IV. The full development of the inversion scheme based on the WSA is part of the authors' ongoing research work.

ACKNOWLEDGMENTS

This work is supported by the University of Illinois Research Board. The authors would like to thank Dr. S.-H. Chen of MIT for insightful discussions.

[1] X.-L. Zhou, G. P. Felcher, and S.-H. Chen, Physica B **173**, 167 (1991).
[2] X.-L. Zhou, S.-H. Chen, and G. P. Felcher, J. Phys. Chem. **95**, 9025 (1991).
[3] X.-L. Zhou, S.-H. Chen, and G. P. Felcher, in *Inverse Problems in Scattering and Imaging,* edited by M. Bertero and E. R. Pike (Hilger, Bristol, 1991), pp. 109–130.
[4] X.-L. Zhou, S.-H. Chen, and G. P. Felcher, Phys. Rev. A **46**, 1839 (1991).
[5] A. Ishimaru, *Wave Propagation and Scattering in Random Media* (Academic, New York, 1978), p. 71.
[6] G. H. Vineyard, Phys. Rev. B **26**, 4146 (1982).
[7] L. D. Landau and E. M. Lifshits, *Quantum Mechanics,* 3rd ed. (Pergamon, New York, 1977), pp. 164–189.
[8] G. Parratt, Phys. Rev. **95**, 359 (1954).
[9] B. E. Warren, *X-Ray Diffraction* (Addison-Wesley, Reading, MA, 1969).
[10] J. Als-Nielsen, Z. Phys. B **61**, 411 (1985).
[11] S.-H. Chen, X.-L. Zhou, and B. L. Carvalho, Prog. Colloid Polym. Sci. **93**, 85 (1993).
[12] X.-L. Zhou, L.-T. Lee, S.-H. Chen, and R. Strey, Phys. Rev. A **46**, 6479 (1992).
[13] G. P. Felcher, A. Karim, and T. P. Russell, J. Non-Cryst. Solids **131-133**, 703 (1991).
[14] R. F. Harrington, *Field Computation by Moment Method* (Macmillan, New York, 1988).